Available online at www.sciencedirect.com

jmr&t Journal of Materials Research and Technology

journal homepage: www.elsevier.com/locate/jmrt

Original Article

# Characterization of Inconel 718® superalloy fabricated by wire Arc Additive Manufacturing: effect on mechanical properties and machinability

*Unai Alonso* [a,*], *Fernando Veiga* [b], *Alfredo Suárez* [b,c], *Alain Gil Del Val* [b]

[a] *University of the Basque Country (UPV/EHU), Department of Mechanical Engineering, Bilbao, Spain*
[b] *TECNALIA, Basque Research and Technology Alliance (BRTA), Parque Científico y Tecnológico de Gipuzkoa, Donostia-San Sebastián, E20009, Spain*
[c] *ADDILAN Fabricación Aditiva S.L., Eguzkitza 1, Durango, 48200, Spain*

ARTICLE INFO

*Article history:*
Received 23 June 2021
Accepted 26 July 2021
Available online 6 August 2021

*Keywords:*
WAAM
Inconel 718
Microstructure
Machinability
Bending moment

ABSTRACT

Wire and Arc Additive Manufacturing has the potential to become an appropriate technique to produce large complex-shaped metallic parts. However, a post-processing machining operation is necessary to reach the final geometry.

In this work, Inconel 718 walls were manufactured in a monitored environment and their microstructure and mechanical properties were characterised. Then, slot milling operations were performed to investigate the influence of cutting speed and machining direction. The conclusions drawn from this article can be used as a guide for a correct definition of strategies and milling parameters. It was observed that at higher cutting speeds a better surface quality and lower torques are obtained. Moreover, the main novelty of this work is that is shows the influence of the anisotropy of WAAM-Inconel 718 on its machinability. Milling along the torch's travel direction offers better dimensional tolerance values with lower cutting torques, being more favourable than machining in the building direction.



## 1. Introduction

INCONEL 718 (IN718) is a hardenable nickel-based superalloy with a service temperature in the range from 16 K to 977 K. This alloy exhibits an excellent oxidation resistance, high tensile and fatigue strength, and good creep behaviour. Since its development in the 1960s, its use has spread in several industrial sectors and it can be found in hot sections of aircraft turbines, nuclear reactor parts or drilling equipment for oil and gas exploration. The manufacturing of complex geometries in IN718 is challenging due to its bad machinability, and fixing worn parts is also a difficult task [1,2]. For this reason, it is necessary to develop manufacturing processes that reduce the amount of wasted material, enhance design freedom and are more cost-effective.

The interest in producing IN718 components using additive manufacturing (AM) techniques has grown remarkably in the last decade (including laser powder bed fusion or laser direct

* Corresponding author.
E-mail address: unai.alonso@ehu.eus (U. Alonso).
https://doi.org/10.1016/j.jmrt.2021.07.132

metal deposition, among other processes [1–4]). AM techniques which use metal powder as a raw material often give rise to porosities and unmelted particles which shorten the parts' life [5,6]. Hot isostatic pressing (HIP) has proven to be a solution to these issues, but it leads to bigger grain sizes and lower mechanical properties [6]. Furthermore, part quantity and size are also limited by the low deposition rate (0,12–0,6 kg/h) [7]. These disadvantages can be overcome with the use of Wire Arc Additive Manufacture (WAAM). This AM process uses a welding wire as the feedstock and plasma or an electric arc as the heat source. As compared to other techniques, WAAM is outstanding due to its higher deposition rate (1–8 kg/h), it has lower equipment costs and is more environmentally-friendly [8,9].

WAAM can be performed using three main types of welding technologies: metal inert gas (MIG), tungsten inert gas (TIG) and plasma arc welding (PAW). The main advantage of MIG is that the wire (used as a consumable electrode to form the arc) is positioned coaxially to the welding torch and permits higher freedom of movement. This technology is also known as gas metal arc welding (GMAW) and is the most frequently used one. On the contrary, TIG and PAW use non-consumable electrode and the filler wire is added sideways between the electrode and the workpiece. A recent MIG variant named cold metal transfer (CMT) provides accurate heat input using a high frequency wire feeding system and has been reported to provide weld beads of high quality and low thermal damage for several alloys [9–11].

Research work developed so far on IN718 alloy manufactured by WAAM has been focused on the understanding of the metallurgical microstructure and its relationship with the mechanical and chemical properties. Xu et al. systematically studied the effects of oxide and heat treatment on mechanical properties of WAAM IN718 [12]. Their results showed that a 0.5 μm thick passivation layer (consisting of $Cr_2O_3$ and $Al_2O_3$) is formed upon deposition and it prevents further oxidation of the material inside the bulk. They also observed large columnar grains and numerous Laves phase, as compared to the finer grains obtained by laser powder bed fusion. This starting microstructure led to less precipitates during the heat treatment and a lower average strength than in the wrought alloy.

The incorporation of interpass cold rolling to the process can prevent the generation of such large columnar grains. Xu et al. observed that plastic deformation induced by rolling triggers a non-uniform recrystallization upon successive depositions [13]. The structure formed by small columnar and numerous finely equiaxed grains allowed more precipitation at the grain boundaries, improved aging response, and led to a mechanical strength 75 MPa higher than the wrought standard. However, residual Laves and δ phase were found in the heat-treated WAAM IN718 and their effect is not clear yet.

Van et al. demonstrated that in-situ heat treatment during deposition is possible using CMT-based WAAM approach [10]. Successive depositions were carried out using continuous heat from a plasma arc and the interpass time was varied. The authors also observed a columnar dendrite microstructure along the entire sample length, with exception of the top layer. Moreover, an aging effect was detected for the first-time using deposition with CMT. Strengthening phases such as γ'' and γ' were developed and contributed to a higher microhardness in the middle section of each deposit. In a recent work, Kindermann et al. [14] investigated the effect of deposition and heat treatment parameters employed on CMT-WAAM. Their results show that, as travel speed increased, Laves length and carbide diameter decreased; while a rise on as-deposited hardness was noticed. Besides, an increase in the solution treatment temperature from 980 to 1040 °C reduced microsegregation, Laves and δ phase precipitation. The authors also observed that the arc stability considerably decreases for widths over 10 mm.

In order to reach a high level of printing resolution, a good control of the bead width, weld cap reinforcement and penetration depth are required. Benakis et al. [15] studied the capacity of a single Pulsed-GTAW system to produce a variety of bead geometries in WAAM IN718 by using both high and low frequency pulsing. Apart from the pulsing modes, the effect of the variation torch travel speed as well as the wire-feeding rate were also evaluated. Their results demonstrate that high frequency pulsing leads to a lower heat input and to the constriction of the arc, reducing the heat affected zone. Besides, the variation of speed and wire-feed enable them to create both high penetration/wide beads as well as low penetration/narrow beads.

Despite the possibility of generating beads of a wide variety of sizes with high deposition rates, WAAM workpieces have poorer dimensional accuracy and surface finish as compared to other AM processes [16]. IN718 parts are used in components subjected to thermo-mechanical cyclic stresses, in which surface integrity plays a major role in the nucleation of cracks. Thus, it is necessary to perform machining post-processing operations that improve the part's properties [17].

So far, IN718 machining research has focused on parts made with powder-based processes [18–20]. Calleja et a [18]. compared the machinability of IN718 in three different states of the material: manufactured by Laser Metal Deposition (both at not heat-treated and heat-treated conditions) and wrought (heat treated). Higher cutting forces and poorer surface finish were registered for both hardened AM and wrought workpieces due to their higher hardness. Similar conclusions were also reported by Ostra et al. in a recent study [19].

The path followed during the AM process has a great influence on the metallurgical microstructure of the part, on its mechanical properties, as well as its machinability. In this regard, Körner et al. [20] showed that scanning strategies in selective electron beam melting can produce an IN718 columnar grain structure with a high texture in building direction or a complete texture-free fine-grained structure. Fei et al. [21] investigated the effect of build direction and scanning strategy on the machinability of IN625. Their result revealed that the milling strategy (along or perpendicular to the deposition direction) has a major influence on chip formation and milling forces. In addition, Park et al. [22] observed that the relative position between the machining and deposition paths has more effect on tool wear than the difference in hardness. However, no works have been found in the literature that analyse this effect in the machining of WAAM IN718.

Even if WAAM could be a viable alternative to manufacturing aerospace components, there are no studies that investigate the machinability of IN718 produced by WAAM technology. This work aims to analyse both the influence of material properties and the cutting speed in a slot-milling operation. During the tests, machinability properties such as cutting forces and surface roughness values will be evaluated. It has also been shown in literature that the anisotropy of the deposited material can condition the machining process. Thus, microstructural characteristics and mechanical properties of the parts will be studied for a deeper understanding of the deposition process.

## 2. Experimental setup

The experimental procedure performed in this study consisted of two stages: (i) the analysis of the WAAM process, in which the characterization of the IN718 properties was carried out, along with (ii) the study of slot milling operations in the fabricated part. Fig. 1 shows an overview of the experimental procedure, exhibiting both the steps and the techniques utilized for their characterization, which are further detailed in the next sections.

### 2.1. *Fabrication of IN718 parts via WAAM*

Two IN718 walled structures were produced with Plasma Arc Welding (PAW) based WAAM approach. In the first one, the resulting metallurgical microstructure and the mechanical properties were analysed and the second one was used for milling tests.

An Addilan V0.1. tilt table machine was used for the deposition of the IN718 WAAM walls (see Fig. 1). This machine-tool is equipped with a Tetrix 552 AC/DC Synergic Plasma EWM AG power source for automated applications and can reach deposition rates up to 6 kg/h. Besides, it also incorporates an oxygen concentration sensor, an Optrics pyrometer and a QuellTech Q4 laser profilometer (which was used to measure the wall height).

The material for the manufacturing of the walls consisted of an IN718 wrought plate with a thickness of 10 mm and a wire with a diameter of 1.2 mm. The chemical composition of both the substrate and the feedstock material is presented in Table 1.

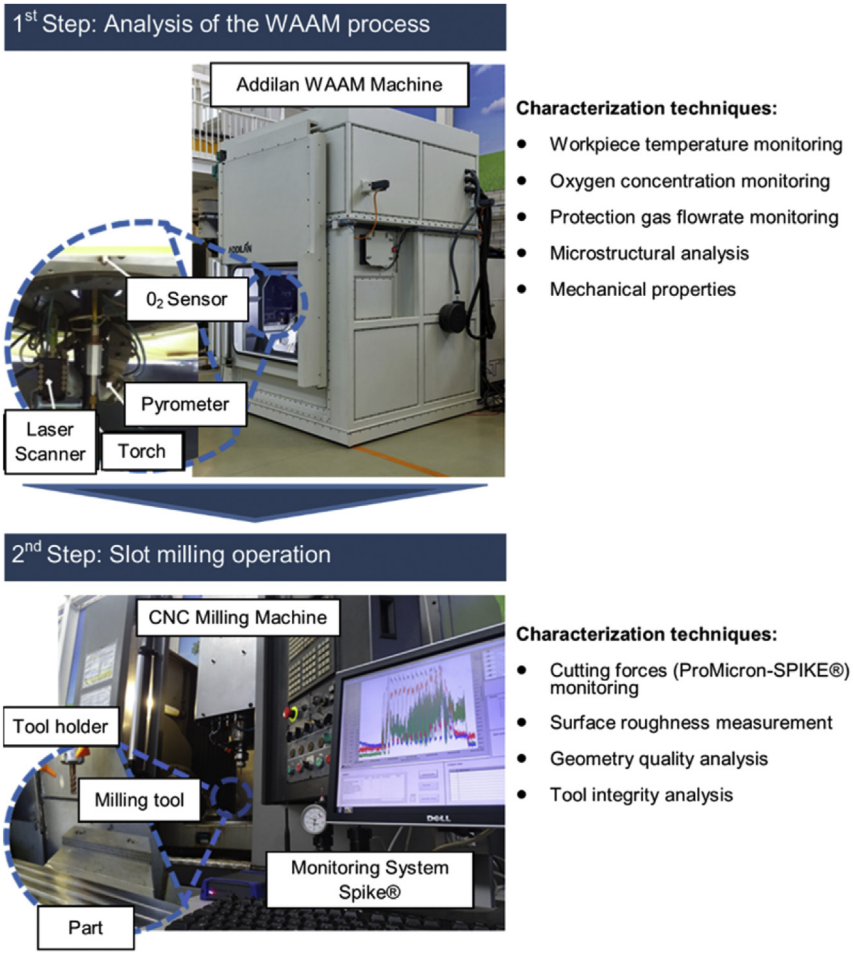


**Fig. 1 – Conceptual view of the approach taken during the experimental work.**

**Table 1 – Chemical composition of the wrought plate (substrate) and the IN718 wire.**

| Alloy/Wt.% | Ni | Cr | Nb + Ta | Mo | Ti | Al | Co | Mn | Fe |
|---|---|---|---|---|---|---|---|---|---|
| Substrate | 53.5 | 18.67 | 5.01 | 2.9 | 0.94 | 0.58 | 0.22 | 0.09 | 17.9 |
| Wire | 52.3 | 18.81 | 5.33 | 3.2 | 0.96 | 0.53 | 0.35 | 0.15 | Bal. |

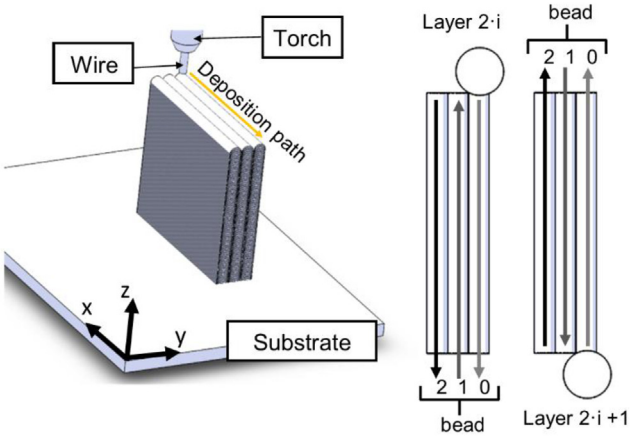


**Fig. 2 – Schematic process sequence for wall manufacturing.**

As shown in Fig. 2, the WAAM process was carried out using a switchback stroke strategy and the deposition direction was inverted at the end of each weld to compensate non-uniform growth of the layer. Each layer consisted of the interposition of three beads with an overlapping distance of 65% of the width of the bead. The alternating layers were deposited in opposite directions in order not to lose geometric tolerance until the desired wall height was reached. Moreover, an interpass cooling strategy (ICT) was implemented with a wall surface temperature set at 300 °C. This temperature was chosen to maintain the quality of the parts without incurring excessive time penalties. Argon was used both as a plasma and shielding gas. A flow rate of 12 l/min was used to protect the welding area from the environment and the oxygen level was maintained under 50 ppm.

Table 2 shows the process parameters used for the manufacturing of the walls. Among the different parameters, the energy-related ones are especially relevant to study the melting rate of both the wire and the base material. Melting energy can be estimated quantitatively based on the equation of Specific Heat Capacity and is expressed as:

$$E_m = m \cdot c_p \cdot (T_m - T_0) \quad (1)$$

where $c_p$ is the heat capacity of IN718 (approximately 0.435 J/(g °K)), $T_f$ is the melting temperature (1573 K) and $T_0$ is room temperature. The mass of the deposited layer ($m$ in Eq. (1)) can be estimated from Eq. (2) based on the density $\rho$ (8.19 g/cm$^3$) and on the wire diameter ($D_w$).

$$m = \rho \cdot \pi \cdot \left(\frac{D_w}{2}\right)^2 \quad (2)$$

The energy supplied to the wire for each millimetre travelled ($E_d$), as well as the amount of energy deposited ($E_w$) can be obtained by Eqs. (3) and (4) respectively. These parameters have been estimated from the average values of current and voltage and considering the nominal values of forward speed and wire speed. Finally, The Melting Ratio can be obtained by Eq. (5). The parameter combination listed in Table 2 was selected because it allows obtaining sufficient arc energy to melt the wire material.

$$E_d = I \cdot V / TTS \quad (3)$$

$$E_w = I \cdot V / WFS \quad (4)$$

$$MR = E_m / E_w \quad (5)$$

### 2.2. *Slot milling experiments*

After deposition of the wall, the upper and lower part of the piece were cut. As can be seen in the works by Van and Lopes [1,2], the substrate acts as a heat sink, giving rise to a metallurgical microstructure different from the one obtained in the centre of the piece. In this zone, the resulting microstructure can be stabilized by following a controlled interpass cooling strategy (ICS) [1]. Therefore, the temperature in the bead was monitored by pyrometry and an ICS strategy was followed with a cooling time between passes of 180s. The dimensions of the resulting specimen were 60 × 60 × 20 mm.

In the case of IN718 deposited by WAAM the metallurgical grains are columnar and this could affect the cutting forces depending on the milling direction selected [21]. To study the influence of machining direction, tests were carried out both

**Table 2 – Process parameters for the manufacturing of the IN718 WAAM walls.**

| Current, I [A] | Voltage V [V] | Torch Travel Speed, TTS [mm/min] | Wire Feed Speed, WFS [m/min] | Deposition Rate, DR [kg/h] |
|---|---|---|---|---|
| 180 | 20 | 230 | 2.5 | 1.39 |
| Melting Energy, Em [J/mm] | | Wire Energy, Ew [J/mm] | Deposition Energy, Ed [J/mm] | MR [J/J] |
| 5.1 | | 86.4 | 939 | 0.06 |

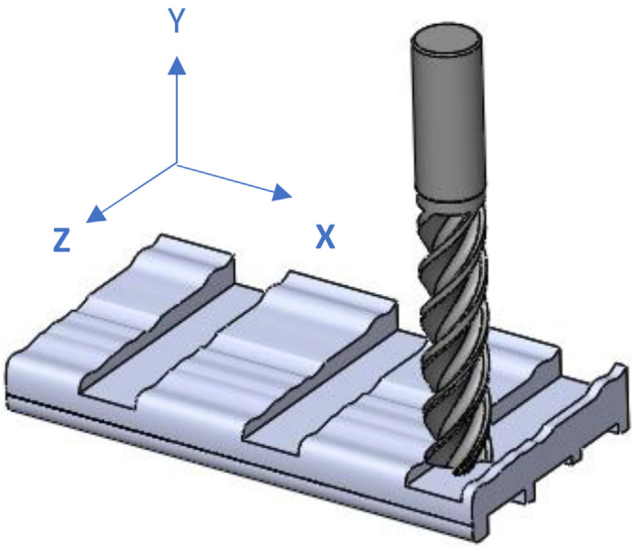


**Fig. 3 – Milling operations along the IN718 WAAM part.**

along the travel direction (X axis) and building direction (Z axis) (see Fig. 3). The cutting tools used were micro-grain carbide end mills with 10% of cobalt binder, $D = 10$ mm, 4 flutes, unequal helix angles (42°–45°) and TiAlN coating. The slot milling operations were performed on a five-axis machining centre (Ibarmia 5-axis ZV 65/U600 EXTREME).

Table 3 shows the studied machining parameter combinations. These were chosen according to previous experiences and performing adjustment tests to obtain a stable cutting process. Besides, Minimum Quantity Lubrication (MQL) was selected as coolant. This type of refrigeration is being adopted more and more in the industry as it is more environmentally friendly.

### 2.3. *Characterization techniques*

To observe the microstructural changes that took place during plasma arc welding, the samples were cross-sectioned, mounted, ground, and polished for further analysis. Standard polishing procedures were used for general microstructural observations (40 mL of hydrochloric acid and 3 mL of $H_2O_2$). Microstructures of the weld metal, heat-affected zone (HAZ) and fusion boundary were studied with an optical microscope (OM). The microstructures were also characterized using scanning electron microscopy (SEM, JEOL JSM-5910LV).

**Table 3 – Slot milling parameters.**

| Parameter | Machining conditions |
|---|---|
| Milling tool | TiAlN coated carbide end mill. |
| No. of teeth. | 4. |
| Cutting speed | 40, 50, 60 m/min |
| Feed per toot | 0,066 mm/rev |
| Axial depth of cut | 0.5 mm |
| Radial depth of cut | 10 mm |
| Coolant | Minimum quantity lubrication (MQL): 30 mL/h |

As shown in Fig. 4, tensile test cylindrical specimens with a 4 mm diameter body were also extracted along the travel (X) and building direction (Z) to check the effect of directionality (see Fig. 1). Furthermore, on the regions where the slot milling operations were performed, the microhardness was determined using a Future-Tech FM-800 Hardness Testing Machine with a load of 0.5 kg applied for 10 s.

During the slot milling tests, thrust force, cutting torque and tool bending moments were registered using a sensory SPIKE® toolholder (Pro-micron GmbH, Kaufbeuren, Germany) wirelessly connected to a PROMICRON READ acquisition system. Afterwards, force signals were treated using the software MATLAB Signal Analyzer. The 3D surface of the machined surfaces was registered using a Leica DCM 3D microscope. Then the average surface roughness (Ra) was measured with the LeicaMaps prost-processing software in accordance with ISO 4288 standard. Besides, slot width was also analysed with a Mitutoyo inside micrometre caliper (resolution: 0,01 mm, maximum permissible error ±5 μm).

## 3. Results

### 3.1. *Microstructural characterization*

Microstructure analysis was carried out in the central part of the wall in the YZ plane and Fig. 5a shows the interface between wall and substrate. Columnar grain grew epitaxially in the opposite direction to the heat flow, and crystal growth proceeded in the Z axis. A coaxial grain structure was noticeable at the wrought substrate. Among them, there is a transition region identified as “heat affected zone” (HAZ). During the deposition of the first layer, there is no accumulated heat and this layer experiences a higher cooling rate than those on top of it. As a result, a finer microstructure is generated at the interface as compared to that of the wall core.

Figs. 5 and 5c show the central area of the wall with a different magnification number. A fine columnar dendrite structure without secondary dendrites can be noticed and grain boundaries (indicated with red arrows) are also observed. Lave phases and MC carbides were also identified in the interdendritic region as shown in the SEM image in Fig. 5d. The formation of these phases is caused by the segregation of refractory elements Nb and Mo in the nonequilibrium solidification conditions [23]. Besides, no hot cracking was detected in the studied samples. This phenomenon is usually found in this type of additive manufacturing process due to heating cycles with little downtime between layers [24].

Fig. 6 shows optical microscope (OM) macrographs taken along the travel and building directions. A columnar grain structure was observed in the YZ plane as a result of the epitaxial growth due to the directional heat flow. Remelting zones in the Z direction could also be identified in the macrograph. The remelting area was developed in the upper part of the solidified weld during the deposition of the following layer. For the case of the XZ plane, the grain distribution at the edges of the part where the machining was carried out was predominantly equiaxial.

Previous works [10,25] have shown that the columnar grain size is not uniform along the entire height of the wall and this

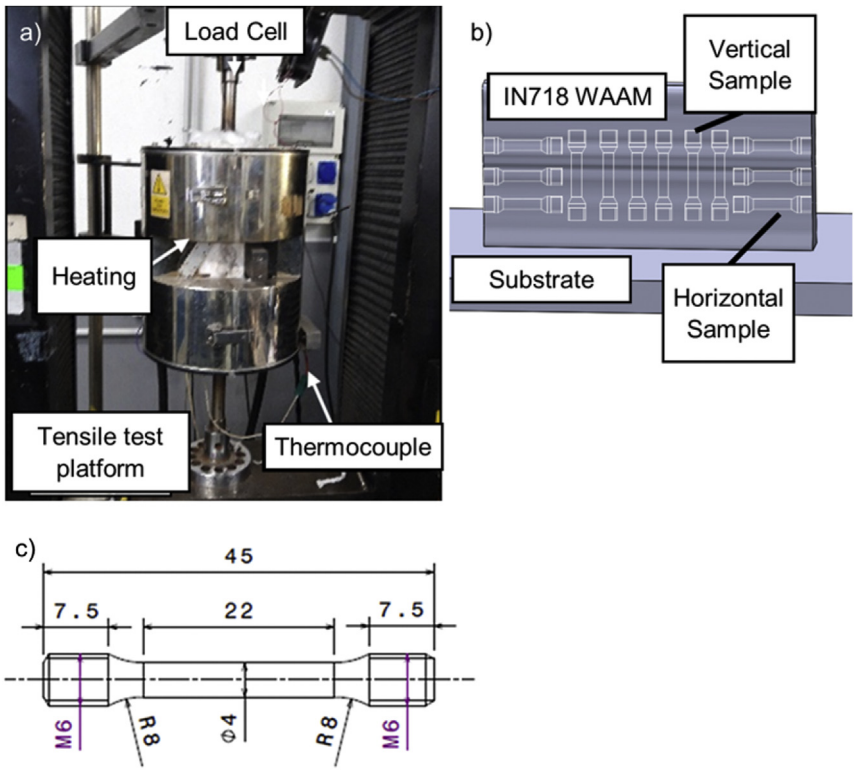


**Fig. 4 – (a) Tensile test platform, (b) Schematic representation of the location of the specimens; (c) Dimensions of the test specimen.**

can affect the mechanical properties and machinability of the part. For the subsequent study of the milling of WAAM IN718, the central area of the wall (in which there is a more uniform grain size) was selected.

### 3.2. *Mechanical properties*

Table 4 lists some mechanical properties of the WAAM IN718 walls both at room and at high temperature (650C). IN718 is

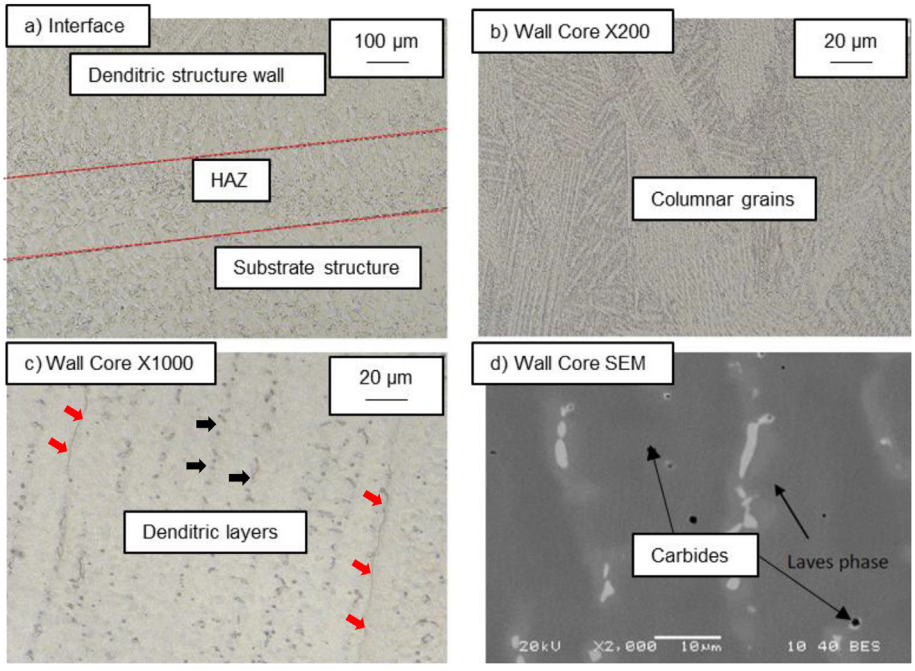


**Fig. 5 – a) OM images of the interface microstructure (substrate-HAZ-wall), b) columnar grains at the wall core, c) dendritic layers formation at the wall core and d) SEM analysis of the INCO 718 microstructure carbides and laves phases formation.**

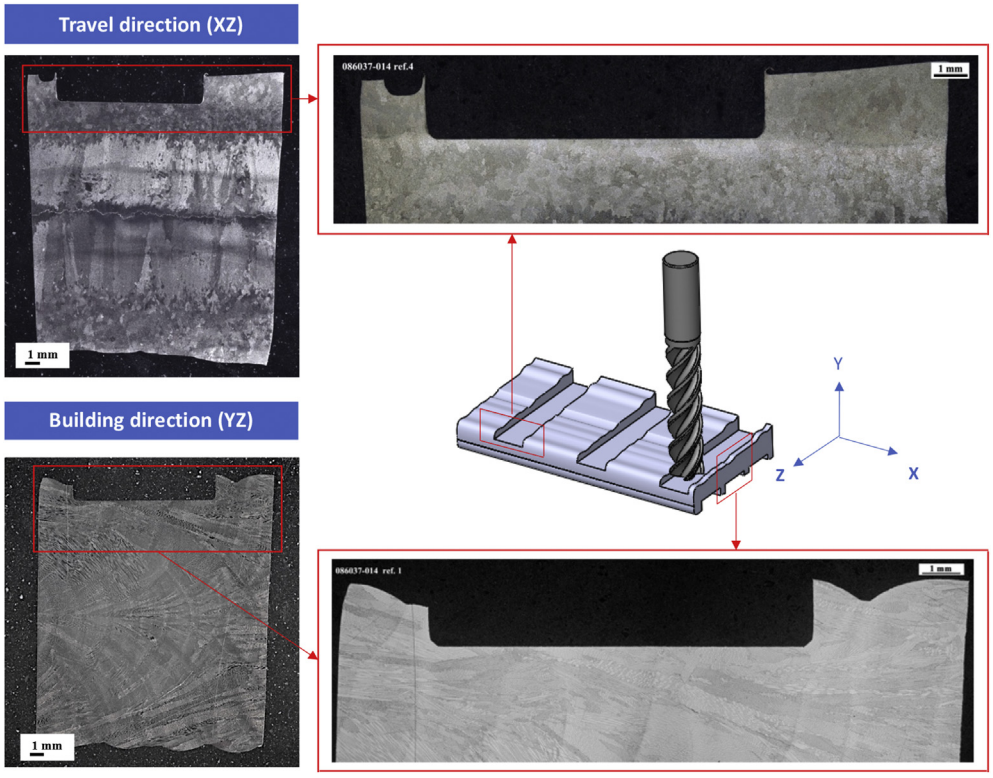


**Fig. 6 – OM macrographs of the samples in the travel and building direction.**

generally used in aircraft engines and turbine blades in this temperature range [26]. During the machining process, such high temperature values can also be reached both in the workpiece and the cutting tool surface [27].

Yield strength was considerably higher in the case of WAAM manufactured alloy as compared to a non-treated cast workpiece. This result can be linked to the finer grain structure obtained by the high cooling rates of this additive manufacturing method. Moreover, tensile and yield strengths of the specimens were slightly higher in the travel direction (X axis) than those in the building direction (Z axis). Besides, Fig. 7 compares the results of the tensile test for the studied loading directions and temperatures. Both anisotropy and mechanical properties cloud be further improved by a combination of interpass rolling strategy followed by an aging treatment [12].

The microhardness tests carried out along the building direction showed very similar values (250 ± 4HV). This uniformity can be linked to the stability in the microstructure which is favored by the interpass cooling strategy (ICT). Fig. 8 shows the

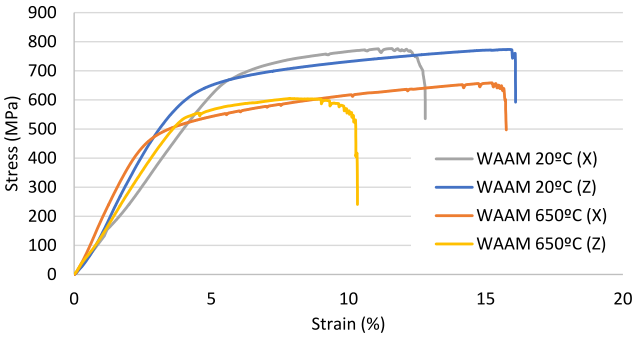


**Fig. 7 – Stress–strain curves for the studied loading directions and temperatures.**

temperature registered by the pyrometer during the deposition of the layers 2 to 12. After the deposition of each layer, heat on the surface of the weld decreases rapidly due to the thermal conduction to the rest of the wall and substrate. Afterwards,

**Table 4 – Mechanical properties from tensile testing of IN718 WAAM manufactured wall.**

| Test Temperature | Loading Direction | Yield strength (MPa) | Tensile strength (MPa) | Elongation (%) |
|---|---|---|---|---|
| WAAM (20 °C) | Travel direction (X) | 537.2 ± 22 | 774.8 ± 90 | 13.5 ± 7 |
| | Building direction (Z) | 494.4 ± 25 | 773.4 ± 25 | 16.1 ± 5 |
| WAAM (650 °C) | Travel direction (X) | 463 ± 35 | 652.6 ± 80 | 14.5 ± 10 |
| | Building direction (Z) | 444 ± 25 | 605.6 ± 40 | 8.5 ± 5 |
| Casting (20 °C) [28] | | 352 | 607 | 39,4 |

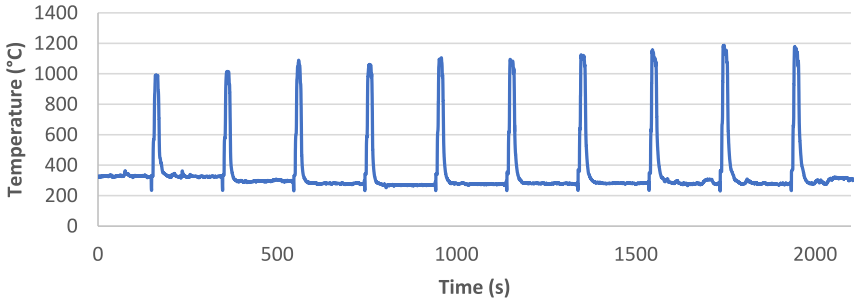


**Fig. 8 – Temperature registered by the pyrometer during the deposition of layers 2 to 12.**

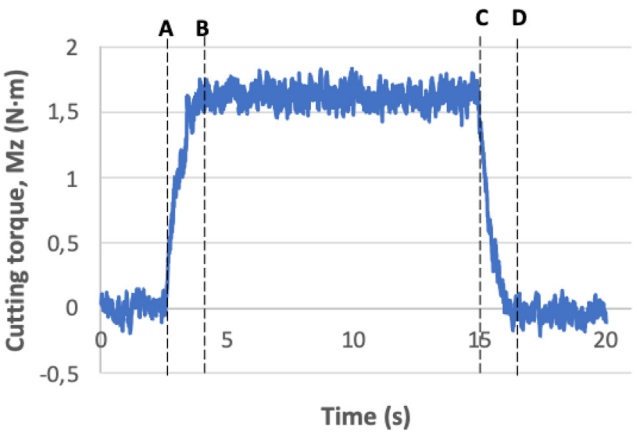


**Fig. 9 – Cutting torque signal evolution during a slot milling test.**

the evaluation of heat is slower since the main means of evacuation is the convection in the outer surface of the wall. For the studied material and workpiece geometry, it was observed that a time between passes of 180 s was sufficient to keep the part at a set temperature of around 300 C. The effect that the variation of interpass time has on the hardness distribution can be observed in the work Van et al. [10].

### 3.3. *Milling tests results*

The particularities of the material's microstructure and the fact that its mechanical properties are not isotropic make it especially interesting to study its machinability. The following sections show the results concerning cutting forces, surface roughness and dimensional quality.

#### 3.3.1. *Cutting forces*

Fig. 9 depicts the cutting torque signal during a slot milling test after applying a low-pass filter. As it can be observed, the evolution of the cutting torque is composed of three stages. The first one (A ➡ B) corresponds to the entry of the milling cutter in the workpiece and the cutting torque grows steadily from zero. In the second one (B ➡ C), the tool is completely engaged, and the cutting torque shows a stable evolution. The irregular peaks on the signal can be linked to two aspects: the variation of the uncut chip thickness and the small vibrations caused by the adhesion of IN718 during chip removal. Finally, the third stage (C ➡ D) it is related to the output from the part. The existence of 3 stages were also observed in the evolution of the bending moment signals in the X and Y axes of the milling cutter. For the study of the influence of the cutting speed and the machining direction, the mean values in the second stage were considered.

Fig. 10a shows the variation of the mean cutting torque force with cutting speed and machining direction. It can be observed that the cutting torque decreases with the increase of cutting speed for both the tests performed along the travel direction (X axis) and building direction (Z axis). This result may be attributed to the following reasons. First, increasing cutting speed leads to a rise in the temperature of the cutting zone easing plastic deformation. Besides, friction in the tool-chip boundary is also reduced and milling is done at a lower cutting force. Similar results were also observed for the tool's bending moment (see Fig. 10b).

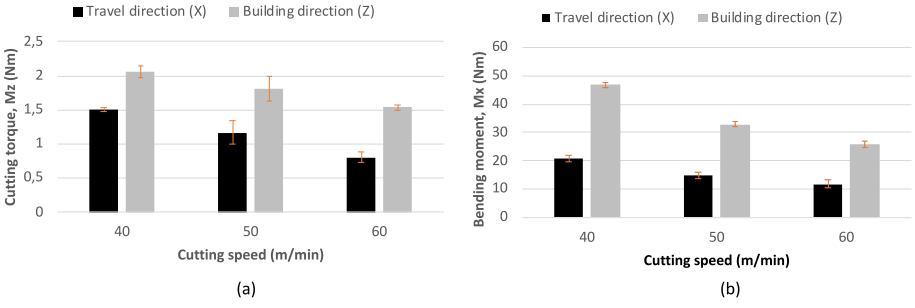


**Fig. 10 – (a) Influence of cutting speed and machining direction on the cutting torque. (b) Influence of cutting speed and machining direction on the bending moment.**

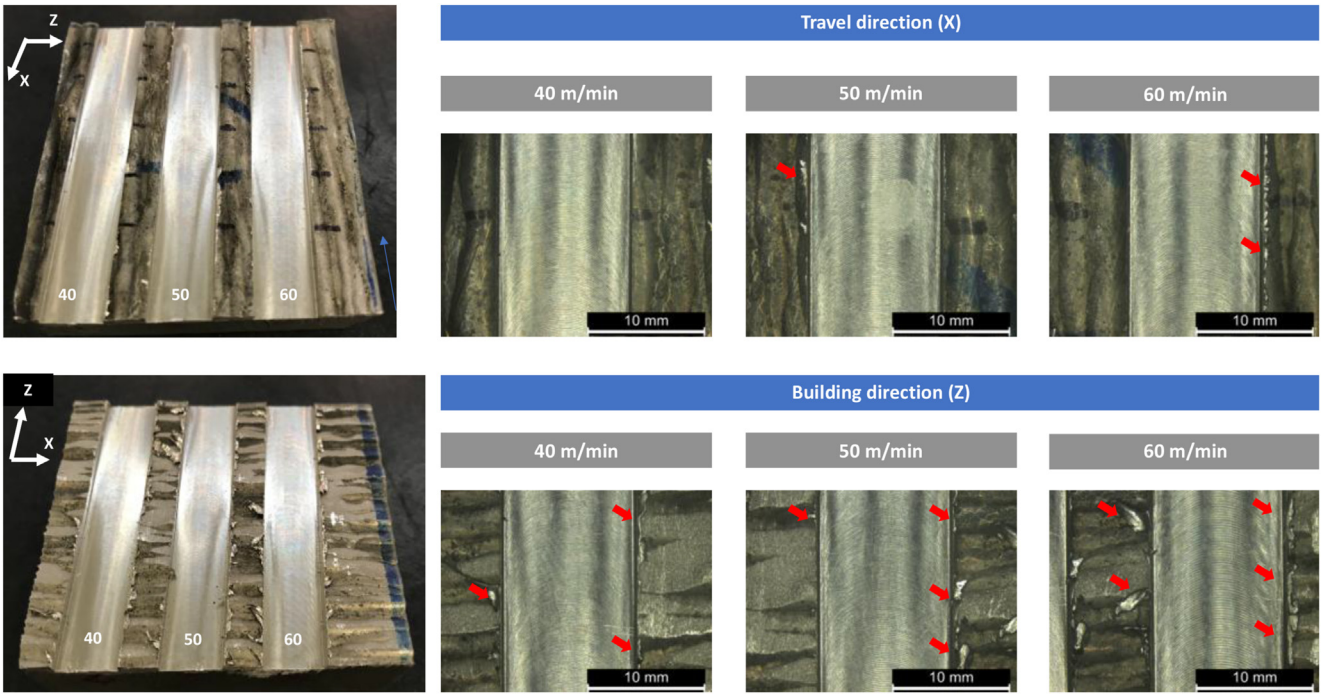


**Fig. 11 – Occurrence of burrs on the machined grooves.**

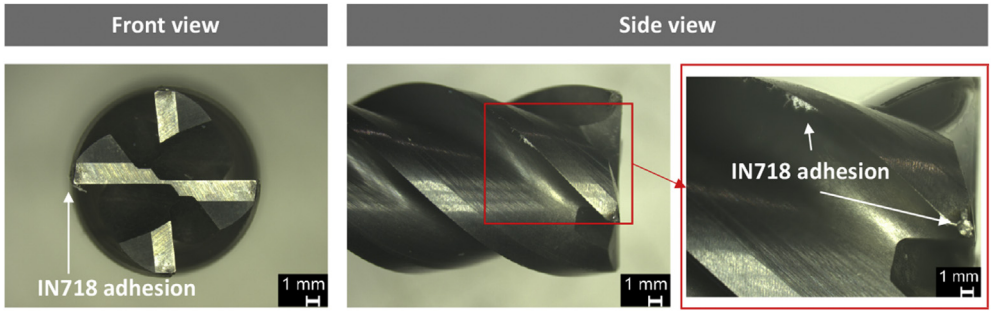


**Fig. 12 – Tool state after machining a slot (Vc = 60 m/s; machining direction: Z axis).**

The increase in cutting temperature favored the appearance of top burrs in the grooves. This defect results from massive plastic deformation during the compression of the tool against the workpiece. Consequently, a portion of the material flows towards the sides of the active cutting edge, instead of being removed. As shown in Fig. 11, the increase in cutting speed caused this type of defect to be more noticeable. Workpiece material adhesion was also detected at the cutting edges after machining (see Fig. 12). The higher ductility of IN718 also provided the conditions for this wear mode.

Furthermore, differences were also observed depending on the milling direction. As shown in Fig. 10, cutting forces were lower when machining along the travel direction (X axis). This variation in workpiece machinability can be correlated to the higher yield strength of WAAM IN718 in this direction. These results are in accordance with the observations made by Fei et al. [21] for a IN718 part manufactured by laser powder bed fusion. In this work, the authors even suggest the possibility of using different tool geometries depending on the selected machining direction.

### 3.3.2. *Surface roughness and dimensional quality analysis*

Surface roughness has a significant role in stress corrosion resistance, creep strength and fatigue life. Thus, it is an important factor in assessing the capability of machining performance. Fig. 13a shows the influence of cutting speed and machining direction on average surface roughness parameter (Ra) during milling of WAAM IN718. The values shown represent the average of three measurements made at three equally spaced positions along the path of the groove.

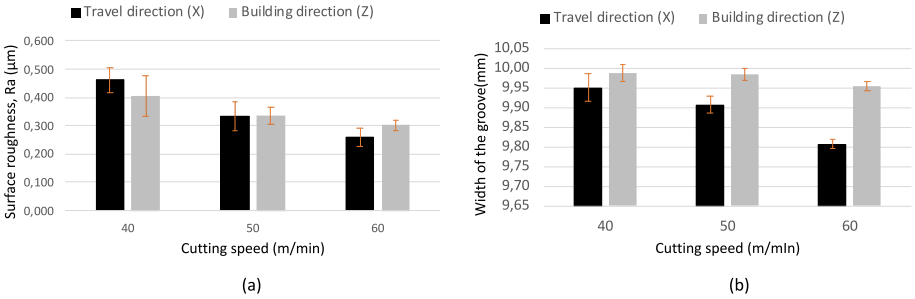


**Fig. 13 – Influence of cutting speed and machining direction on: (a) average surface roughness parameter (Ra); (b) width of the groove.**

Meanwhile, the error bars correspond to the maximum and minimum values obtained in the measurements. The roughness profiles and 3D topographies measured in the center of the grooves are also shown in Fig. 14.

Results showed that roughness values decrease by increasing the cutting speed. This trend is a consequence of an easing in plastic deformation during chip removal due to temperature rise between tool nose and the chip. Additionally, the sticky nature of IN718 at low cutting speeds makes it more difficult for the chips to detach from the workpiece. No significant differences were observed between the grooves made in travel direction as compared to those in the building direction.

Finally, Fig. 13b shows the results of the dimensional analysis of the grooves. As with the roughness measurements, 3 measurements were taken along the tool path. For both machining directions, an increase in cutting speed led to narrower grooves. This phenomenon could be seen as a result of the lower bending moment experienced by the tool in X axis. In fact, comparing Figs. 13b and 10b, the evolution

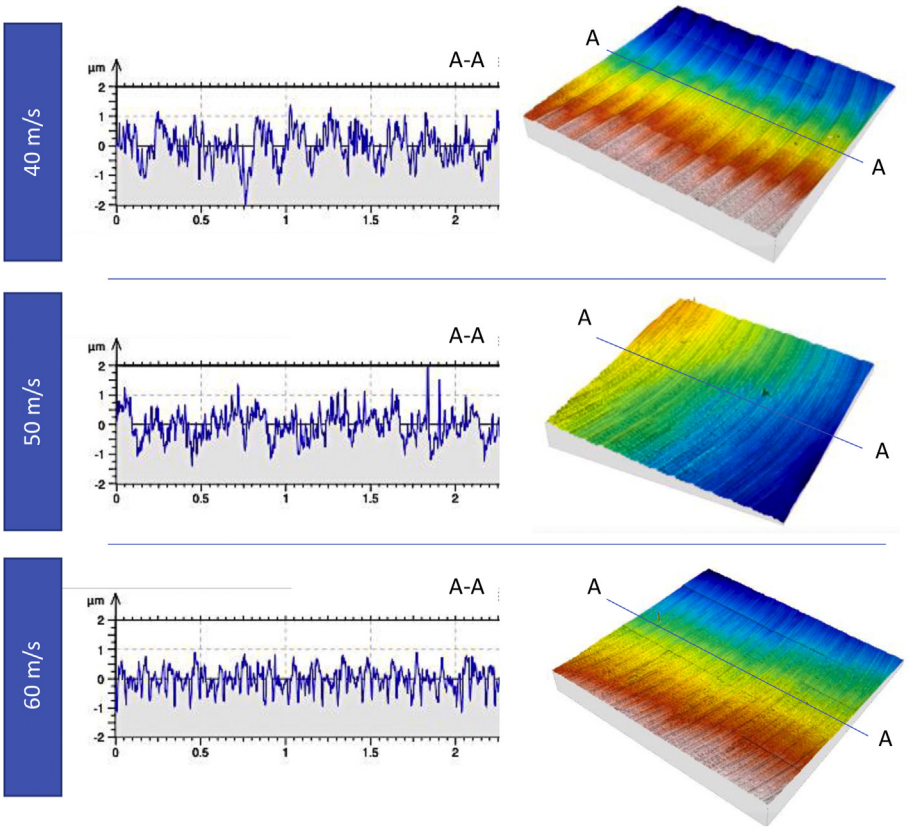


**Fig. 14 – The roughness profiles and 3D topographies measured in the center of the grooves (Machining in building direction).**

of the groove width follows the same trend as the bending moment.

## 4. Conclusions

In this work, the deposition process and mechanical properties of INCONEL 718 produced by Wire Arc Additive Manufacturing were studied. The machinability of the resulting material was also evaluated by slot milling tests. Based on the experimental results, the following major conclusion were drawn:

- A fine dendrite microstructure was generated during the WAAM manufacturing process. A columnar grain distribution was observed in the building plane (YZ) as a result of the directional heat flow, while it was predominantly equiaxial at outer surface in the deposition plane (XZ). Lave phases and carbides where also identified in the interdendritic region and were caused by nonequilibrium cooling conditions.
- Mechanical properties of the WAAM alloy were better than those of the as-cast alloy and comparable to other WAAM methods with cold metal transfer process. However, yield and tensile strengths were higher in the travel direction (X axis) than those in the building direction (Z axis). This mechanical anisotropy may be related to the lower cutting torque and bending moments observed when machining in the building direction.
- Machining forces decreased as cutting speed increased. This effect can be explained by the easing in plastic deformation due to the higher temperatures during chip removal.
- Typical defects from milling, such as top burrs were also observed and were more noticeable at higher cutting speeds. Moreover, the surface roughness improved with the increase of cutting speed regardless of the machining direction. Within the studied cutting parameters, the best average surface roughness (Ra = 0.258 μm) was obtained when milling with the highest cutting speed (60 m/min) in the building direction.
- Narrower groves were obtained with the increase of cutting speed. This result could be linked to the lower bending moment experienced by the tool in the direction perpendicular to its forward motion.

## Declaration of Competing Interest

The authors declare that they have no known competing financial interests or personal relationships that could have appeared to influence the work reported in this paper.

## Acknowledgment

The authors acknowledge the Basque Government for financing the HARIPLUS, HAZITEK 2019 program (ZL-2019/00352) and QUALYFAM project [kk-2020/00042]. The authors are also thankful to the Basque government for supporting the Basque university group on Advanced manufacturing ref: IT1337-19.

## REFERENCES

[1] Aydinöz ME, Brenne F, Schaper M, Schaak C, Tillmann W, Nellesen J, et al. On the microstructural and mechanical properties of post-treated additively manufactured Inconel 718 superalloy under quasi-static and cyclic loading. Mater Sci Eng, A 2016;669:246–58. https://doi.org/10.1016/j.msea.2016.05.089.

[2] Popovich VA, Borisov EV, Popovich AA, Sufiiarov VS, Masaylo DV, Alzina L. Functionally graded Inconel 718 processed by additive manufacturing: crystallographic texture, anisotropy of microstructure and mechanical properties. Mater Des 2017;114:441–9. https://doi.org/10.1016/j.matdes.2016.10.075.

[3] Huang W, Lin X. Research progress in laser solid forming of high-performance metallic components at the state key laboratory of solidification processing of China. 3D Print Addit Manuf 2014;1:156–65. https://doi.org/10.1089/3dp.2014.0016.

[4] Dhinakaran V, Ajith J, Fathima Yasin Fahmidha A, Jagadeesha T, Sathish T, Stalin B. Wire Arc Additive Manufacturing (WAAM) process of nickel based superalloys-A review. Mater Today Proc 2020;21:920–5. https://doi.org/10.1016/j.matpr.2019.08.159.

[5] Jia Q, Gu D. Selective laser melting additive manufacturing of Inconel 718 superalloy parts: densification, microstructure and properties. J Alloys Compd 2014;585:713–21. https://doi.org/10.1016/j.jallcom.2013.09.171.

[6] Zhong C, Gasser A, Kittel J, Wissenbach K, Poprawe R. Improvement of material performance of Inconel 718 formed by high deposition-rate laser metal deposition. Mater Des 2016;98:128–34. https://doi.org/10.1016/j.matdes.2016.03.006.

[7] Liberini M, Astarita A, Campatelli G, Scippa A, Montevecchi F, Venturini G, et al. Selection of optimal process parameters for Wire Arc additive manufacturing. Procedia CIRP 2017;62:470–4. https://doi.org/10.1016/j.procir.2016.06.124.

[8] Wu B, Pan Z, Ding D, Cuiuri D, Li H, Xu J, et al. A review of the wire arc additive manufacturing of metals: properties, defects and quality improvement. J Manuf Process 2018;35:127–39. https://doi.org/10.1016/j.jmapro.2018.08.001.

[9] Derekar KS. A review of wire arc additive manufacturing and advances in wire arc additive manufacturing of aluminium. Mater Sci Technol 2018;34:895–916. https://doi.org/10.1080/02670836.2018.1455012.

[10] Van D, Dinda GP, Park J, Mazumder J, Lee SH. Enhancing hardness of Inconel 718 deposits using the aging effects of cold metal transfer-based additive manufacturing. Mater Sci Eng, A 2020;776:139005. https://doi.org/10.1016/j.msea.2020.139005.

[11] Gu J, Cong B, Ding J, Williams SW, Zhai Y. Wire and Arc additive manufacturing of aluminum. 25th annu int solid free fabr symp austin. 2014. p. 451–8. TX, USA.

[12] Xu X, Ding J, Ganguly S, Williams S. Investigation of process factors affecting mechanical properties of INCONEL 718 superalloy in wire + arc additive manufacture process. J Mater Process Technol 2019;265:201–9. https://doi.org/10.1016/j.jmatprotec.2018.10.023.

[13] Xu X, Ganguly S, Ding J, Seow CE, Williams S. Enhancing mechanical properties of wire + arc additively manufactured INCONEL 718 superalloy through in-process thermomechanical processing. Mater Des 2018;160:1042–51. https://doi.org/10.1016/j.matdes.2018.10.038.

[14] Kindermann RM, Roy MJ, Morana R, Prangnell PB. Process response of Inconel 718 to wire + arc additive manufacturing with cold metal transfer. Mater Des 2020;195:109031. https://doi.org/10.1016/j.matdes.2020.109031.
[15] Benakis M, Costanzo D, Patran A. Current mode effects on weld bead geometry and heat affected zone in pulsed wire arc additive manufacturing of Ti-6-4 and Inconel 718. J Manuf Process 2020;60:61–74. https://doi.org/10.1016/j.jmapro.2020.10.018.
[16] Ding D, Pan Z, Cuiuri D, Li H. Wire-feed additive manufacturing of metal components: technologies, developments and future interests. Int J Adv Manuf Technol 2015;81:465–81. https://doi.org/10.1007/s00170-015-7077-3.
[17] Flynn JM, Shokrani A, Newman ST, Dhokia V. Hybrid additive and subtractive machine tools - research and industrial developments. Int J Mach Tool Manufact 2016;101:79–101. https://doi.org/10.1016/j.ijmachtools.2015.11.007.
[18] Calleja A, Urbikain G, González H, Cerrillo I, Polvorosa R, Lamikiz A. Inconel®718 superalloy machinability evaluation after laser cladding additive manufacturing process. Int J Adv Manuf Technol 2018;97:2873–85. https://doi.org/10.1007/s00170-018-2169-5.
[19] Ostra T, Alonso U, Veiga F, Ortiz M, Ramiro P, Alberdi A. Analysis of the machining process of inconel 718 parts manufactured by laser metal deposition. Materials 2019;12. https://doi.org/10.3390/ma12132159.
[20] Körner C, Helmer H, Bauereiß A, Singer RF. Tailoring the grain structure of IN718 during selective electron beam melting. MATEC Web Conf 2014;14. https://doi.org/10.1051/matecconf/20141408001.
[21] Fei J, Liu G, Patel K, Özel T. Effects of machining parameters on finishing additively manufactured nickel-based alloy inconel 625. J Manuf Mater Process 2020;4. https://doi.org/10.3390/jmmp4020032.
[22] Park E, Kim DM, Park HW, Park Y Bin, Kim N. Evaluation of tool life in the dry machining of inconel 718 parts from additive manufacturing (AM). Int J Precis Eng Manuf 2020;21:57–65. https://doi.org/10.1007/s12541-019-00275-x.
[23] Zhang J, Zhang X, Wang X, Ding J, Traoré Y, Paddea S, et al. Crack path selection at the interface of wrought and wire + arc additive manufactured Ti-6Al-4V. Mater Des 2016;104:365–75. https://doi.org/10.1016/j.matdes.2016.05.027.
[24] Artaza T, Alberdi A, Murua M, Gorrotxategi J, Frías J, Puertas G, et al. Design and integration of WAAM technology and in situ monitoring system in a gantry machine. Procedia Manuf 2017;13:778–85. https://doi.org/10.1016/j.promfg.2017.09.184.
[25] Artaza T, Bhujangrao T, Suárez A, Veiga F, Lamikiz A. Influence of heat input on the formation of laves phases and hot cracking in plasma arc welding (PAW) additive manufacturing of inconel 718. Metals 2020;10:1–17. https://doi.org/10.3390/met10060771.
[26] Schafrik RE, Ward DD, Groh JR. Application of alloy 718 in GE aircraft engines: past, present and next five years. Proc Int Symp Superalloys Var Deriv 2001;1:1–11. https://doi.org/10.7449/2001/superalloys_2001_1_11.
[27] Kitagawa T, Kubo A, Maekawa K. Temperature and wear of cutting tools in high-speed machining of Inconel 718 and Ti-6Al-6V-2Sn. Wear 1997;202:142–8. https://doi.org/10.1016/S0043-1648(96)07255-9.
[28] El-Bagoury N, Matsuba T, Yamamoto K, Miyahara H, Ogi K. Influence of heat treatment on the distribution of Ni 2Nb and microsegregation in cast inconel 718 alloy. Mater Trans 2005;46:2478–83. https://doi.org/10.2320/matertrans.46.2478.